



PECULIAR STATIONARY EUV WAVE FRONTS IN THE ERUPTION ON 2011 MAY 11

R. CHANDRA¹, P. F. CHEN², A. FULARA¹, A. K. SRIVASTAVA³, AND W. UDDIN⁴¹ Department of Physics, DSB Campus, Kumaun University, Nainital—263 001, India; rchandra.ntl@gmail.com² School of Astronomy & Space Science, Nanjing University, Nanjing—210 023, China³ Department of Physics, Indian Institute of Technology (BHU), Varanasi—221 005, India⁴ Aryabhata Research Institute of Observational Sciences, Manora Peak, Nainital—263 002, India

Received 2015 July 31; accepted 2016 February 25; published 2016 May 12

ABSTRACT

We present and interpret the observations of extreme ultraviolet (EUV) waves associated with a filament eruption on 2011 May 11. The filament eruption also produces a small B-class two ribbon flare and a coronal mass ejection. The event is observed by the *Solar Dynamic Observatory* with high spatio-temporal resolution data recorded by the Atmospheric Imaging Assembly. As the filament erupts, we observe two types of EUV waves (slow and fast) propagating outwards. The faster EUV wave has a propagation velocity of $\sim 500 \text{ km s}^{-1}$ and the slower EUV wave has an initial velocity of $\sim 120 \text{ km s}^{-1}$. We report, for the first time, that not only does the slower EUV wave stop at a magnetic separatrix to form bright stationary fronts, but also the faster EUV wave transits a magnetic separatrix, leaving another stationary EUV front behind.

Key words: Sun: corona – Sun: coronal mass ejections (CMEs) – waves

1. INTRODUCTION

As the two largest eruptive phenomena in a solar atmosphere, both solar flares and coronal mass ejections (CMEs) are frequently associated with erupting filaments, which later become the core of the CMEs. These three phenomena are the three important ingredients in the standard CSHKP model (Carmichael 1964; Sturrock 1966; Hirayama 1974; Kopp & Pneuman 1976) for a flare/CME. In this unified model, the erupting filament plays a very crucial role (Chen 2011).

The erupting filament also drives wave phenomena in the solar atmosphere, which are manifested in radio, $H\alpha$, extreme ultraviolet (EUV), and other wavelengths. In contrast to $H\alpha$ Moreton waves which occur sparsely, the frequently accompanied waves that can be directly imaged are EUV imaging telescope (EIT) waves. EIT waves were discovered in the EUV difference images with the EIT (Delaboudinière et al. 1995) on board the *Solar and Heliospheric Observatory (SOHO)*, Domingo et al. 1995) by Moses et al. (1997) and Thompson et al. (1998). This is the reason why they were named EIT waves more than 17 years ago. Later, several other names were invented for this phenomenon, such as EUV waves and large-scale coronal propagating fronts (Nitta et al. 2013). EIT waves were initially proposed to be the coronal counterparts of $H\alpha$ Moreton waves, i.e., fast-mode magnetohydrodynamic (MHD) waves in the solar corona (Thompson et al. 1998; Wang 2000; Wu et al. 2001). However, these waves present some features which cannot be easily explained by the fast-mode wave model. For example, according to Klassen et al. (2000), the typical velocity of EIT waves is in the range of $170\text{--}350 \text{ km s}^{-1}$, which is about 3 or more times slower than Moreton waves. In some cases, the EIT wave speed can be as small as $\sim 10 \text{ km s}^{-1}$ (Zhukov et al. 2009). In order to resolve the velocity discrepancy, several non-wave models have also been proposed (Gallagher & Long 2011; Chen & Fang 2012; Patsourakos & Vourlidas 2012; Liu & Ofman 2014). For more reviews on EUV waves, see Warmuth (2007), Wills-Davey & Attrill (2009), Zhukov & Veselovsky (2007), Zhukov (2011), Warmuth & Mann (2011), and Patsourakos & Vourlidas (2012). Very recently Warmuth (2015) presented a very

excellent review on the globally propagating coronal waves. The review is focussed on various observational findings, physical nature, and different models of EUV waves proposed in the past years. It seems now that there should be two types of EUV waves with different velocities, and the EIT wave initially discovered by Moses et al. (1997) and Thompson et al. (1998) may correspond to the slower type of EUV waves (Chen et al. 2002). Following Chen & Fang (2012), we use “EIT waves” for the slower type of EUV waves specifically. Biesecker et al. (2002) did a statistical study of EIT waves observed by *SOHO*/EIT (195 Å) telescope and found that some of the EIT waves have sharp, bright features, which they called “S-waves.” These S-waves may be the signature of Moreton waves. They also concluded that EIT waves having S-shape signatures are always associated with both flares and CMEs. On the basis of *SOHO*/EIT observations, Zhukov & Auchère (2004) suggested a bimodal characteristic for EIT waves, i.e., including a wave mode and an eruptive mode component. The wave-mode component is a wavelike phenomenon and represented by pure MHD waves. The eruptive-mode component is defined as propagating bright fronts and dimming as a result of successive stretching of field lines during the eruption of CMEs as modeled by Chen et al. (2002). Downs et al. (2012) presented comprehensive observations of the 2010 June 13 EUV wave observed by the *Solar Dynamic Observatory (SDO)*/Atmospheric Imaging Assembly (AIA) in different channels and conducted 3D MHD simulations of CME eruptions and the associated EUV waves. They suggested that the outer component of EUV waves behaves as a fast-mode wave and found that this component later decouples from the associated CME. Their study distinguishes between the wave and non-wave mechanisms of EUV waves.

An even more serious issue that led Delannée & Aulanier (1999) and Delannée (2000) to doubt the fast-mode wave model for the EIT waves is that they found stationary wave fronts in several events. These stationary fronts are found to be located at the magnetic separatrix. Considering that this feature can hardly be accounted for by the fast-mode wave model, they related the stationary EUV front to the opening of the closed magnetic field lines during the CME. The stationary EUV front

was also explained in the framework of the magnetic field line stretching model proposed by Chen et al. (2002). With numerical simulations, Chen et al. (2005, 2006) illustrated how a propagating EIT wave stops at the magnetic separatrix. However, as mentioned by Delannée & Aulanier (1999), although it is unlikely, there is a possibility that the stationary EUV front is an artifact because it might be due to successive wave fronts reaching the same location after ~ 15 minutes, which is the cadence of the EIT observations. With the high cadence of the *SDO/AIA* observation up to 12 s, this issue can be settled conclusively.

With the purpose to better understand the EUV wave and its stationary fronts, in this paper we present our study of the filament eruption event originating between the active regions NOAA 11207 and 11205 on 2011 May 11. The paper is organized as follows: Section 2 describes the instruments and the observational data. The observational view of filament eruption and associated phenomena are investigated in Section 3, and the EUV waves and its stationary fronts are analyzed in Section 4. The discussion of our results is presented in Section 5. Finally, the conclusion is drawn in Section 6.

2. INSTRUMENTATION AND DATA

The Atmospheric Imaging Assembly (AIA, Lemen et al. 2012) on board the *SDO* satellite (Pesnell et al. 2012) observes the full Sun with different filters in EUV and UV spectral lines with a cadence up to 12 s and a pixel size of $''6$. For the current study, we use the AIA 171 Å, 193 Å, and 304 Å data. The high cadence and high spatial resolution of the AIA images allow us to see more details of the filament eruption and the associated EUV waves. To have a better view of EUV waves, we utilize the base difference images by subtracting each image with one from before the eruption. All the images are corrected for the solar differential rotation. For the magnetograms, we use the data observed by the Helioseismic and Magnetic Imager (HMI, Scherrer et al. 2012) on board the *SDO*. HMI measures the photospheric magnetic field of the Sun with a cadence of 45 s and a spatial resolution $1''$.

3. FILAMENT ERUPTION AND THE ASSOCIATED PHENOMENA

On 2011 May 11 the filament under study is located between the active regions NOAA 11207 and NOAA 11205 at N20W60 on the solar disk. It has a length of ~ 150 Mm. To its north, there is another short filament, which shares the same magnetic neutral line. During eruption, only the longer filament erupts. This filament starts to rise at $\sim 02:10$ UT on 2011 May 11. The eruption of the filament is followed by a weak flare. According to *Geostationary Operational Environmental Satellite (GOES)* observations, the flare is classified as B9.0-class. The soft X-ray enhancement starts at around 02:20 UT, peaks at 02:40 UT, and disappears after 03:20 UT. Looking at the spatial evolution of the flare in Figure 1, the flare shows two quasi-parallel ribbons. As the filament moves up, the two ribbons start to separate from each other, as expected from the standard CSHKP model. The ribbons are located on the opposite sides of the magnetic neutral line. The filament eruption is associated with a CME. According to the LASCO CME catalog, the CME appears in the LASCO field of view around 02:48 UT. The CME is a partial halo event with an angular width of 225° . The

speed and the acceleration of the CME are 740 km s^{-1} and 3.3 m s^{-2} , respectively.

In order to see the kinematics of the filament eruption, we create a time–slice diagram using the *SDO/AIA* 304 Å data. The location of the slice is shown in the top-left panel of Figure 2, and the corresponding time–slice plot is displayed in the bottom-left panel, according to which we plot the time evolution of the filament height in the top-right panel of Figure 2. The diamond symbols correspond to the observations, which are nicely fitted by a fourth order polynomial function. The fitted line is overplotted on the observed data. From the height–time plot, we compute the velocity and the acceleration of the erupting filament. The derived values are plotted in the middle and bottom panels in the right column of Figure 2. It is found that velocity varies in the range of $30\text{--}400 \text{ km s}^{-1}$ and the estimated acceleration varies from 0.1 to 1 km s^{-2} .

In many reported cases, filament eruptions often exhibit two distinct phases, i.e., slow and fast rise phases (Chifor et al. 2006; Schrijver et al. 2008; Koleva et al. 2012; Joshi et al. 2013). Interestingly, in our case, the velocity of the erupting filament changes continually, and we cannot divide the evolution into two phases. Such types of eruptions were proposed in the case of the kink instability (Ji et al. 2003; Török & Kliem 2005; Cheng et al. 2012). In this case, the eruption can occur without the need of the slow rise phase with a nearly constant velocity. Therefore, our eruption event may be initiated by the kink instability in the first instance. However, we did not observe the clear number of twists to meet the Kruskal–Shafranov condition for the kink instability (Srivastava et al. 2010).

4. TWO TYPES OF EUV WAVES AND STATIONARY EUV WAVE FRONTS

The filament eruption on 2011 May 11 is associated with EUV waves. The first appearance of the EUV waves is around 02:00 UT. The wave is seen to propagate mostly in the south-west direction. We display the AIA 171 and 193 Å base difference images to see the evolution of the EUV waves in the two rows of Figure 3, respectively. To make the base difference images, a pre-event image at 02:00 UT is subtracted from each observed image. The propagating EUV waves are clearly seen in Figure 3, including a fast-moving EUV wave marked by yellow arrows, and another slowly moving EUV wave indicated by red arrows. The slowly moving EUV wave is followed by coronal dimmings in both wavelengths. Since the coronal dimmings can be observed in different wavelengths, they are mainly due to the depletion of plasma density. Several authors quantitatively calculated the dimmings due to the plasma density depletion using *Yohkoh/SXT* (Sterling & Hudson 1997), *SOHO/EIT* (Zhukov & Auchère 2004) and *STEREO* data (Aschwanden 2009).

To see the kinematics of the EUV waves clearly, we create a time–slice image in AIA 193 Å. As shown in the left panel of Figure 4, the slice is a great circle starting from the flare region. The right panel of Figure 4 displays the time evolution of the 193 Å intensity distribution along the slice. Inspecting the time–slice diagram, we find that there are two types of waves, one is a fast-moving wave and the other is a slowly moving wave. We claim the fast-moving wave as the fast-mode MHD wave, and the slowly moving wave as the EIT wave, as marked by the arrows in the right panel of Figure 4. The speed of the fast-mode wave is $\sim 500 \text{ km s}^{-1}$, which is several times greater

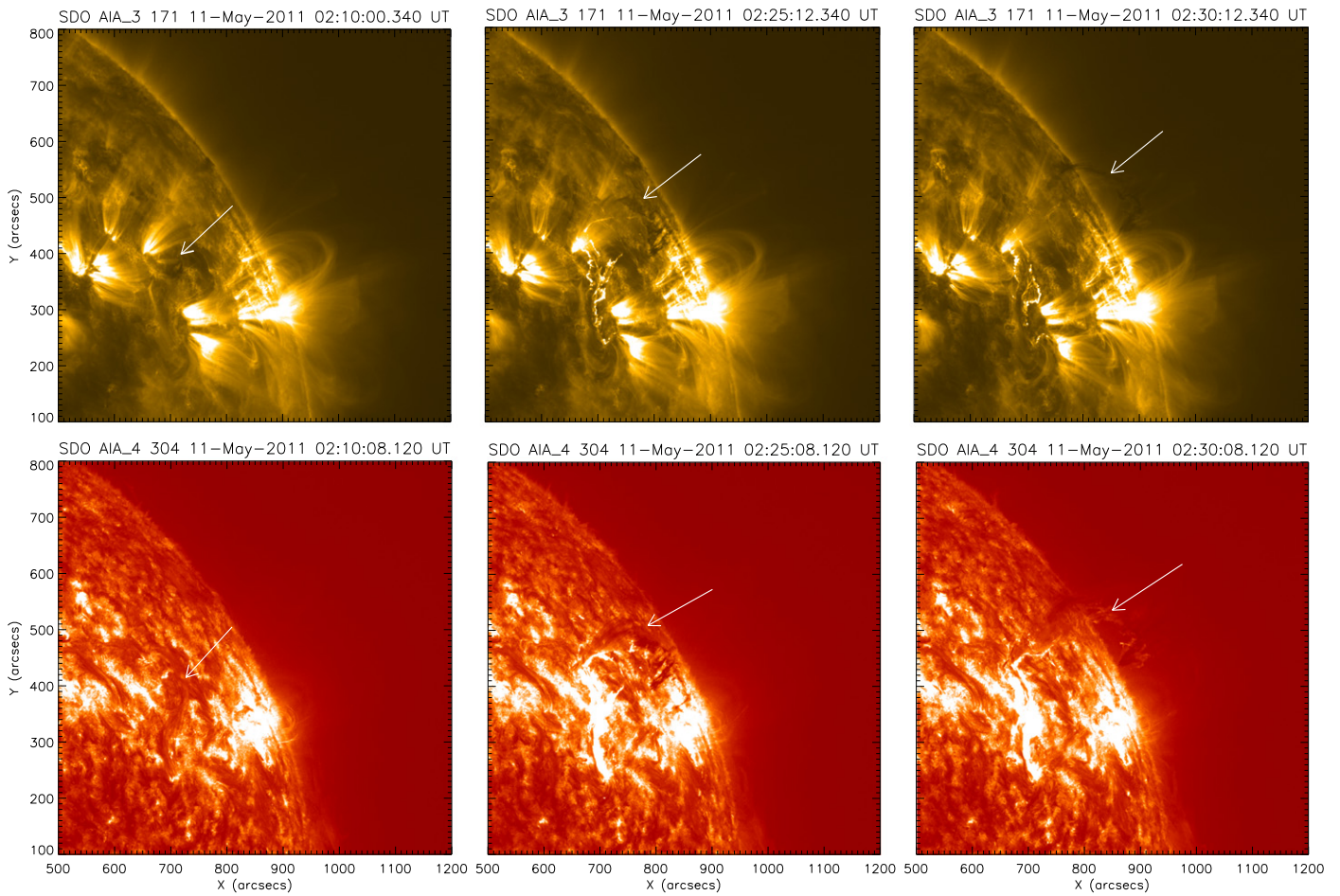


Figure 1. Evolution of the filament eruption followed by the flare observed by *SDO/AIA* in 171 Å and 304 Å, respectively.

than the coronal sound wave. The observed slower wave is a typical EIT wave. The initial speed of the EIT wave is $\sim 120 \text{ km s}^{-1}$, which is even smaller than the coronal sound speed. Note that with the AIA 193 Å formation temperature, the coronal sound speed is 186 km s^{-1} . It is also seen that as time progresses the foremost front of the fast-mode wave keeps a constant speed, whereas the speed of the EIT wave decreases, and around 02:33 UT it stops. Since the EIT wave bifurcates into two fronts, they form two stationary fronts, F_2 and F_3 , at distances of $160''$ and $200''$, respectively. Since the *SDO/AIA* has a 12 s cadence, we can follow the propagation of any EUV waves. It is seen that the stationary fronts at the distances of $160''$ and $200''$ in Figure 4(b) indeed result from the gradual deceleration of the slowly moving EIT waves.

More interestingly, we notice another two stationary fronts in Figure 4(b), which are not related to the EIT waves. The first one, F_1 , is located at a distance of $110''$, and the second one, F_4 , is at a distance of $280''$ in Figure 4(b). The first one, which is very close to the flare site, is the border of a core dimming region. In order to understand the formation of these stationary EUV fronts, we plot the extrapolated coronal magnetic field in Figure 5, where the extrapolation is based on the Potential-Field Source Surface (PFSS) model. After checking the extrapolated magnetic field, we find that Front F_2 (marked by the red line) is nearly cospatial with the magnetic separatrix or quasi-magnetic separatrix layers (QSLs) where magnetic field lines diverge rapidly. Note that a magnetic separatrix is a special case of magnetic QSL, where the neighboring magnetic

fields belong to different magnetic systems. Front F_4 (marked by the yellow line) is not cospatial, but very close to another QSL. Besides, Front F_1 is located inside the magnetic system of the source region, and Front F_3 is shifted slightly from the QSL that is nearly cospatial with Front F_2 .

5. DISCUSSION

When EIT waves were discovered, they were initially considered as fast-mode MHD waves (Thompson et al. 1998; Wang 2000; Wu et al. 2001), i.e., they were the long-awaited coronal counterparts of chromospheric Moreton waves. Moreton waves were discovered by Moreton (1960) and Moreton & Ramsey (1960) as a dark front followed by a bright front in the $H\alpha$ red wing, or a bright front followed by a dark front in the $H\alpha$ blue wing. They have a typical velocity of the order of 1000 km s^{-1} (Smith & Harvey 1971). Despite some apparent evidence that seems to support the fast-mode wave nature of EIT waves (e.g., Ballai et al. 2005; Gopalswamy et al. 2009; Olmedo et al. 2012), a serious problem with the fast-mode wave model is that the EIT wave speed is typically ~ 3 times slower than Moreton waves (Klassen et al. 2000), and in some cases the EIT wave speed is only $\sim 80 \text{ km s}^{-1}$ (Klassen et al. 2000) or even $\sim 10 \text{ km s}^{-1}$ (Zhukov et al. 2009). Nitta et al. (2013) claimed that the large-scale coronal propagating fronts have a mean wave speed of 644 km s^{-1} , which is comparable to that of Moreton waves. However, they always selected the fastest front in each of their time-slice diagrams.

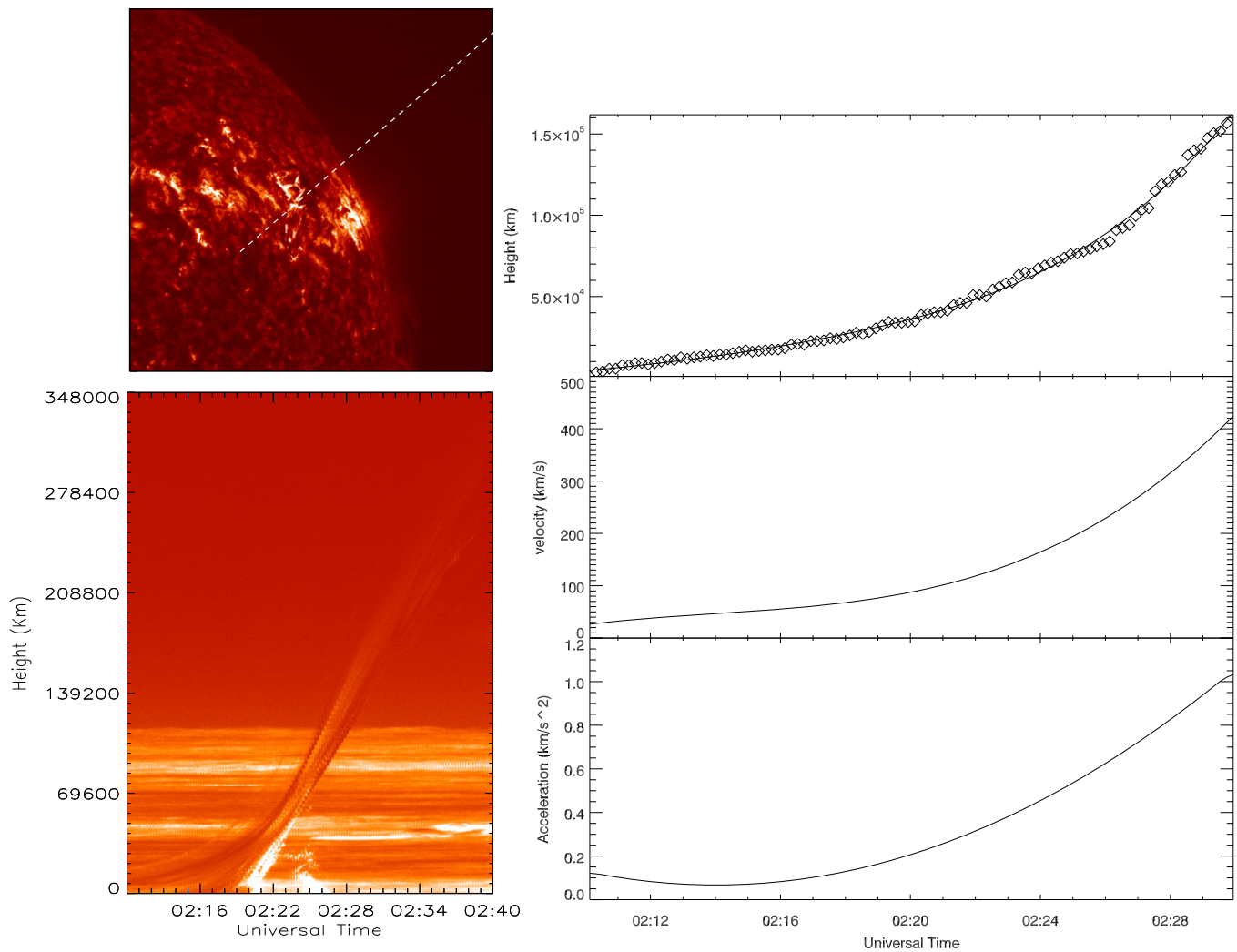


Figure 2. Top left: the *SDO* 304 Å image, where the slice is used to plot the time–distance diagram for the erupting filament; Bottom left: time–slice diagram of the filament eruption; Right top: time evolution of the filament height in observations (diamonds), which is fitted by a fourth order polynomial function (line); Right middle: time evolution of the filament velocity; Right bottom: time evolution of the filament acceleration.

Therefore, in our view, most events in their paper are the coronal counterpart of Moreton waves, rather than the original EIT waves found by Thompson et al. (1998). In our study, whenever we say that the EIT wave is generally three times slower than the fast-mode wave in the corona, we mean the slower one in the two-wave paradigm.

The lack of correspondence between the speeds of Moreton and EIT waves was also suggested by Warmuth et al. (2001, 2004a, 2004b). In order to explain the velocity difference, they proposed that fast-mode wave decelerates from typical Moreton wave speeds to typical EIT wave speeds. Whereas this idea may be able to explain the deceleration of the real fast-mode wave, whose speed is higher, near the source active region than in the quiet region, we definitely need another model to explain those EIT waves whose speeds are below the sound speed. In order to explain the low speeds of many typical EIT waves, Chen et al. (2002, 2005) proposed that two types of EUV waves are formed in association with a filament eruption. The fast-moving wave is a piston-driven shock wave, which corresponds to the coronal counterparts of the chromospheric Moreton waves, and the slow moving wave is an apparent

motion, which is formed due to the successive stretching of the closed magnetic field lines overlying the erupting flux rope.

The co-existence of two types of EUV waves was initially verified by Harra & Sterling (2003), and later conclusively confirmed by the *SDO*/AIA observations (Chen & Wu 2011; Asai et al. 2012; Kumar et al. 2013; White et al. 2013). It can also be identified in many events statistically analyzed by Nitta et al. (2013). As predicted by the magnetic field-line stretching model (Chen et al. 2002), the fast-moving EUV wave is about three times faster than the slow moving EUV wave. For example, the ratio is 2.5 (Harra & Sterling 2003), 2.9 (Chen & Wu 2011), 3.4 (Kumar et al. 2013), and 1.8 (White et al. 2013). In this paper, we also found two EUV waves, with a velocity ratio of 4.2. According to the magnetic field-line stretching model, this relatively large ratio implies that the closed field lines overlying the filament are relatively more stretched in the radial direction. Besides, it is seen that expanding dimmings immediately follow the slower EIT wave, as illustrated by Figure 3. Such a feature is again consistent with the magnetic fieldline stretching model, which interprets that the EIT waves and expanding dimmings are both due to the field line stretching.

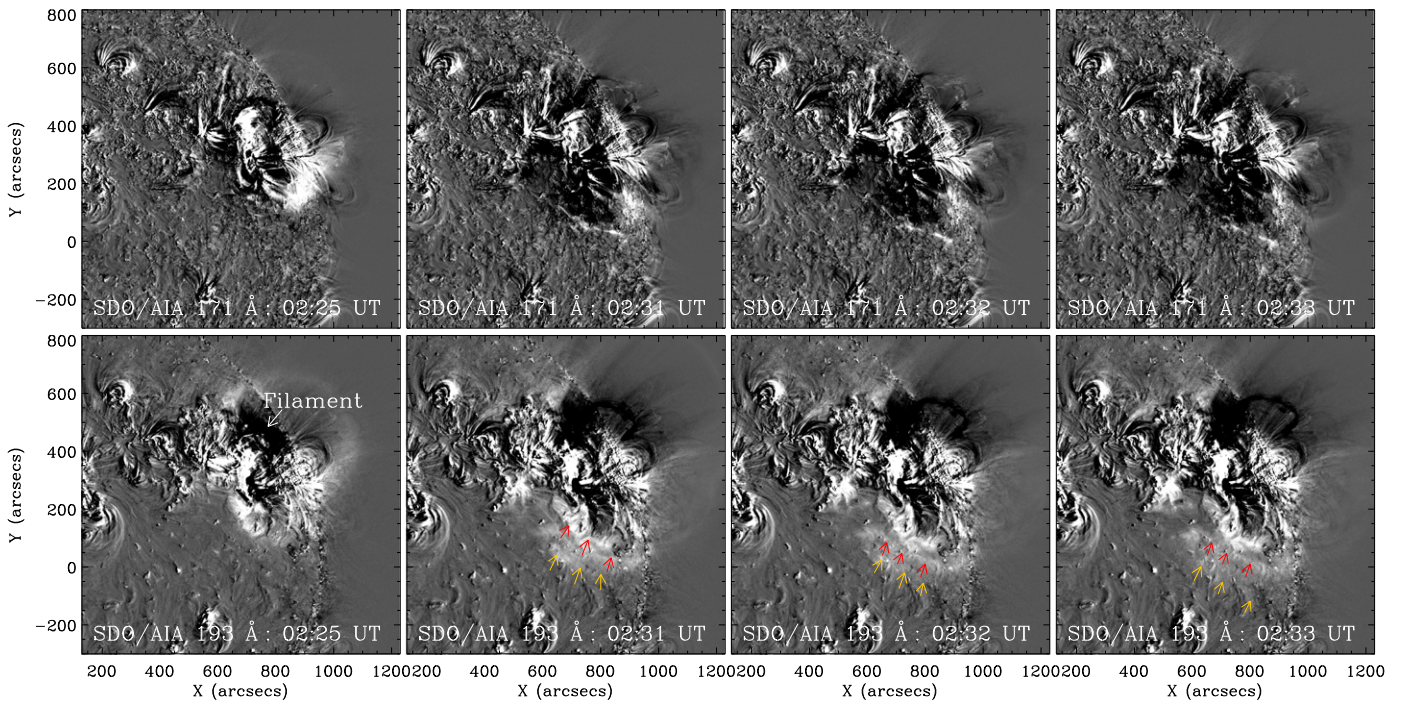


Figure 3. Base difference images of the event observed in *SDO/AIA* 171 and 193 Å. The base image is taken at 02:00 UT. The yellow and red arrows indicate the fast-mode MHD wave and a slowly moving EIT wave, respectively. The white arrow indicates the erupting filament.

(a)

(b)

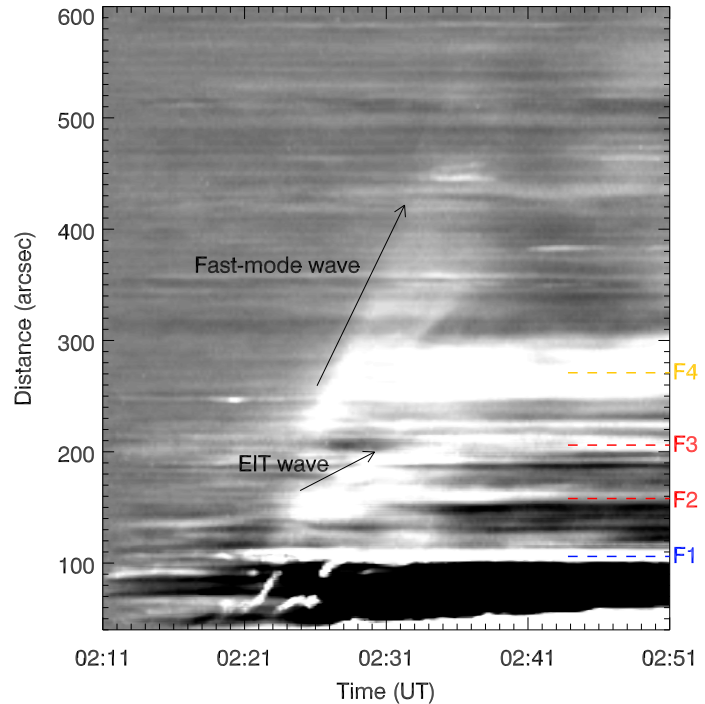
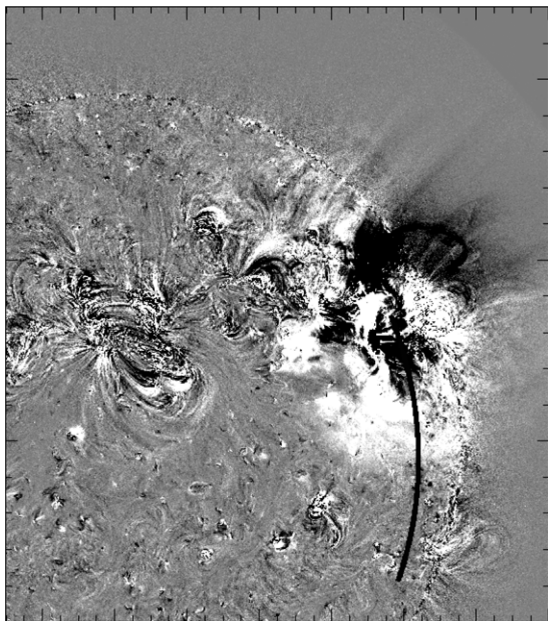


Figure 4. (a) The *SDO/193 Å* (02:11:07 UT) difference image showing a slice (*black line*) to be used in the time–distance diagram. (b) Time–distance diagram showing two types of EUV waves and several stationary fronts, F_1 , F_2 , F_3 , and F_4 . The fast-mode MHD wave and the slowly moving EIT wave are marked by the arrows.

Another feature of EIT waves that led to doubt of the fast-mode wave model is the stationary fronts. Delannée & Aulanier (1999) first reported that an EIT brightening remains at the same location for tens of minutes. They called such brightenings “stationary brightenings.” Later on, such stationary

brightenings were confirmed in several observational studies (Delannée 2000; Attrill et al. 2007; Delannée et al. 2007; Chandra et al. 2009). Such a stationary front located at a magnetic separatrix, or a QSL in more general cases, was reproduced in numerical simulations, and can be explained by

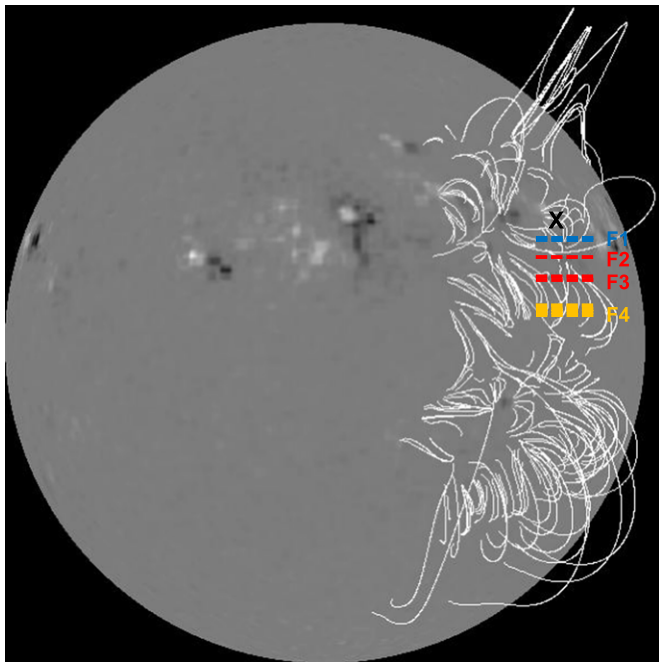


Figure 5. Extrapolated coronal magnetic field using the Potential-Field Source Surface (PFSS) model. The photospheric magnetic field is taken at 00:04 UT observed by HMI on board the *SDO*. The locations of several stationary fronts shown in Figure 4 are overlotted. The black cross indicates the location of the active region.

the magnetic field-line stretching model (Chen et al. 2005, 2006). Despite this, there has still been doubt about the validity of the stationary fronts due to the low cadence of the EIT telescope. With the high cadence observations of the 2011 May 11 event by *SDO/AIA*, we confirm that the slowly propagating EIT wave finally stops at a magnetic QSL. One peculiar feature in this event is that the EIT wave bifurcates into two stationary fronts, F_2 and F_3 in the time–slice diagram (Figure 4), and only the first front, F_2 , is cospatial with a QSL, with the other one being slightly shifted away. These detailed structures cannot be detected with the telescopes before *SDO* was launched. One possibility of the bifurcation is that the outer front is the traditional EIT wave front, whereas the inner front is simply an expanding coronal loop, as proposed by Cheng et al. (2012). Another possibility, which we favor, is that the two fronts are due to the projection of different layers of one EIT wave front since the EIT wave front has a domelike structure in three dimensions (Veronig et al. 2010). In addition to the bifurcation of the slower EUV wave into fronts F_2 and F_3 , even inside front F_3 , a multitude of strands are identifiable. One might wonder whether the fine structures inside front F_3 can be explained by slow-mode shocks, which was proposed by Wang et al. (2009, 2015). With the current observations, we could not tell. As for the Soliton model (Wills-Davey et al. 2007), we are still not sure whether a slow-mode soliton wave can propagate across magnetic field lines and stop at magnetic separatrix. More strikingly, we find two more stationary fronts, F_1 and F_4 , where F_1 is close to the flare site, and F_4 is formed when the fast-mode wave interacts with another magnetic QSL.

It seems from Figure 4 that the stationary front F_1 emanates at $\sim 02:19$ UT, which is slightly earlier than the onset of the solar flare around 02:20 UT. Therefore, it would be more related to the initiation of the filament eruption. It is noticed

that this stationary front is located at the boundary of the core dimmings. Since the core dimmings are generally believed to be due to the evacuation of plasma associated with the erupting flux rope (Sterling & Hudson 1997; Jiang et al. 2003), this stationary front might be formed at the interface between the flux rope (near the footpoint) and the envelope magnetic field (which is more like potential). In this sense, the current shell model proposed by Delannée et al. (2008) may provide a sound explanation for front F_1 .

As for another stationary front F_4 , it seems that it is formed when the fast-mode MHD wave passes through the magnetic QSL at a distance of $280''$ away from the flare site. This feature has never been reported, and generally it is thought that a fast-mode wave may pass through a magnetic QSL freely, leaving no significant traces behind since a magnetic QSL is a topological characteristic, and the magnetic field strength may change smoothly across the QSL.

However, from a theoretical point of view, when a wave propagates in a non-uniform medium, wave reflection would be produced when the intrinsic wave speed of the medium changes rapidly. In particular, when the wave speed in a layer is much lower than that of other regions outside, a wave passing through would be decomposed into a transmitting component and a trapped component that bounces back and forth inside this layer, just like the Fabry–Pérot interferometer. Inspired by the observational result presented in this paper, we (2016, in preparation) call such a layer a “magnetic valley,” and are planning to study how such a magnetic valley responds to an incident wave by numerical simulations. So far a similar phenomenon was numerically investigated by Yuan et al. (2015). Murawski et al. (2001) and Yuan et al. (2015) did a one-dimensional simulation of the propagation of fast magnetoacoustic pulses in a randomly structured plasma and found that the magnetoacoustic pulses were trapped by the randomly structured plasma. Such a “magnetic valley” exists when the QSL is a magnetic separatrix, and the magnetic fields on the two sides of the separatrix belong to two different magnetic systems. The magnetic field around the separatrix might be strongly divergent. In this case, after a fast-mode MHD wave enters this magnetic valley, only a part of the wave can be refracted from the low-Alfvén speed region out to the high-Alfvén speed region, with the remaining part of the wave being trapped in the magnetic valley, bouncing back and forth between the two interfaces. We illustrate this physical process in Figure 6. This observational feature of EUV waves merits further numerical simulations. Unfortunately we cannot identify the bouncing waves at the stationary front. The possible reason is that in two or three dimensions, the magnetic valleys have different widths at different heights, contrary to the one-dimensional case. Therefore, trapped waves with different periods are mixed together in the projected plane, making each wave unidentifiable. It is also noted that, as seen in Figure 5, the stationary front F_4 is not exactly cospatial with the QSL. Such a shift might be due to the limitation of the PFSS model, or such a stationary front is formed with a mechanism different from our conjecture mentioned above.

Kwon et al. (2013) also reported stationary EUV fronts after the passage of a fast-mode shock wave. However, the two fronts in their paper are actually separating in opposite directions with a small velocity. Since the two EUV fronts are located on the two footpoints of a helmet streamer, the brightenings are probably produced by the magnetic

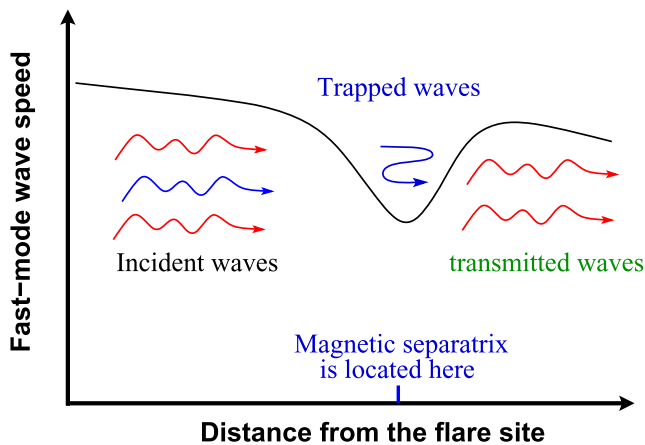


Figure 6. Illustration of physical process for the interpretation of the stationary front F_4 .

reconnection of the current sheet above the helmet streamer triggered by the passing shock wave (B. Vršnak 2016, private communication), which are like flare ribbons and different from ours.

Alternatively, the formation of the stationary front F_4 might be interpreted as stoppage of expansion of structures inside the CME as suggested by Cheng et al. (2012). Cheng et al. (2012) presented the study of formation and separation of two EUV waves from the expansion of a CME. They also reported that the CME and the faster EUV wave propagate with different kinematics after they decouple.

6. CONCLUSIONS

In this study, we presented the observations of two propagating EUV waves, i.e., a fast-mode MHD wave and a slowly moving EIT wave associated with a filament eruption and a CME, as found in many other CME events via the *SDO*/AIA. In association with the two propagating waves, we observed four stationary fronts i.e., F_1 , F_2 , F_3 , and F_4 , as indicated by Figure 4. The stationary wave fronts F_2 and F_3 are the results of the gradual deceleration of the slowly moving EIT wave, which finally stops near the location of a QSL. The formation of Front F_2 can be explained by the magnetic field-line stretching model proposed by Chen et al. (2002, 2005). Front F_3 is bifurcated from front F_2 , so it is shifted slightly away from the QSL. This might be due to the projection effects, i.e., Front F_3 is from a higher layer of the same domelike EIT wave front as Front F_2 .

Front F_1 is proposed to be related to the initiation of the filament eruption and is located at the edge of the core dimmings. This may correspond to the edge of the erupting flux rope at the footpoint. It might be explained by the current shell model proposed by Delannée et al. (2008). Stationary front F_4 is observed for the first time. We tentatively explain it to be formed when the fast-mode MHD wave interacts with a magnetic QSL. During the interaction, a fraction of the wave passes through, with the rest being trapped locally. Other possibilities are not excluded though.

We are thankful to the referee for his/her detailed comments and suggestions, which improved the manuscript significantly. The authors thank the open data policy of the *SDO* team. R.C. and A.F. are supported by the ISRO/RESPOND project no.

ISRO/RES/2/379/12-13, and P.F.C. is supported by the Chinese foundations (NSFC grant nos. 11533005 and 11025314).

REFERENCES

- Asai, A., Ishii, T. T., Isobe, H., et al. 2012, *ApJL*, **745**, L18
- Aschwanden, M. J. 2009, *AnGeo*, **27**, 3275
- Attrill, G. D. R., Harra, L. K., van Driel-Gesztelyi, L., & Démoulin, P. 2007, *ApJL*, **656**, L101
- Ballai, I., Erdélyi, R., & Pintér, B. 2005, *ApJL*, **633**, L145
- Biesecker, D. A., Myers, D. C., Thompson, B. J., Hammer, D. M., & Vourlidas, A. 2002, *ApJ*, **569**, 1009
- Carmichael, H. 1964, *The Physics of Solar Flares*, ed. W. N. Hess (Washington, D. C.: NASA), 451
- Chandra, R., Schmieder, B., Aulanier, G., & Malherbe, J. M. 2009, *SoPh*, **258**, 53
- Chen, P. F. 2011, *LRSRP*, **8**, 1
- Chen, P. F., & Fang, C. 2012, in *EAS Publications Ser. 55*, ed. M. Faurobert, C. Fang, & T. Corbard, 313
- Chen, P. F., Fang, C., & Shibata, K. 2005, *ApJ*, **622**, 1202
- Chen, P. F., Fang, C., & Shibata, K. 2006, *AdSpR*, **38**, 456
- Chen, P. F., Wu, S. T., Shibata, K., & Fang, C. 2002, *ApJL*, **572**, L99
- Chen, P. F., & Wu, Y. 2011, *ApJL*, **732**, L20
- Cheng, X., Zhang, J., Olmedo, O., et al. 2012, *ApJL*, **745**, L5
- Chifor, C., Mason, H. E., Tripathi, D., Isobe, H., & Asai, A. 2006, *A&A*, **458**, 965
- Delaboudinière, J., Artzner, G. E., Brunaud, J., et al. 1995, *SoPh*, **162**, 291
- Delannée, C. 2000, *ApJ*, **545**, 512
- Delannée, C., & Aulanier, G. 1999, *SoPh*, **190**, 107
- Delannée, C., Hochedez, J.-F., & Aulanier, G. 2007, *A&A*, **465**, 603
- Delannée, C., Török, T., Aulanier, G., & Hochedez, J.-F. 2008, *SoPh*, **247**, 123
- Domingo, V., Fleck, B., & Poland, A. I. 1995, *SoPh*, **162**, 1
- Downs, C., Roussev, I. I., van der Holst, B., Lugaz, N., & Sokolov, I. V. 2012, *ApJ*, **750**, 134
- Gallagher, P. T., & Long, D. M. 2011, *SSRv*, **158**, 365
- Gopalswamy, N., Yashiro, S., Temmer, M., et al. 2009, *ApJL*, **691**, L123
- Harra, L. K., & Sterling, A. C. 2003, *ApJ*, **587**, 429
- Hirayama, T. 1974, *SoPh*, **34**, 323
- Ji, H., Wang, H., Schmahl, E. J., Moon, Y.-J., & Jiang, Y. 2003, *ApJL*, **595**, L135
- Jiang, Y., Ji, H., Wang, H., & Chen, H. 2003, *ApJL*, **597**, L161
- Joshi, N. C., Srivastava, A. K., Filippov, B., et al. 2013, *ApJ*, **771**, 65
- Klassen, A., Aurass, H., Mann, G., & Thompson, B. J. 2000, *A&AS*, **141**, 357
- Koleva, K., Madjarska, M. S., Duchlev, P., et al. 2012, *A&A*, **540**, A127
- Kopp, R. A., & Pneuman, G. W. 1976, *SoPh*, **50**, 85
- Kumar, P., Cho, K.-S., Chen, P. F., Bong, S.-C., & Park, S.-H. 2013, *SoPh*, **282**, 523
- Kwon, R.-Y., Ofman, L., Olmedo, O., et al. 2013, *ApJ*, **766**, 55
- Lemen, J. R., Title, A. M., Akin, D. J., et al. 2012, *SoPh*, **275**, 17
- Liu, W., & Ofman, L. 2014, *SoPh*, **289**, 3233
- Moreton, G. E. 1960, *AJ*, **65**, 494
- Moreton, G. E., & Ramsey, H. E. 1960, *PASP*, **72**, 357
- Moses, D., Clette, F., Delaboudinière, J.-P., et al. 1997, *SoPh*, **175**, 571
- Murawski, K., Nakariakov, V. M., & Pelinovsky, E. N. 2001, *A&A*, **366**, 306
- Nitta, N. V., Schrijver, C. J., Title, A. M., & Liu, W. 2013, *ApJ*, **776**, 58
- Olmedo, O., Vourlidas, A., Zhang, J., & Cheng, X. 2012, *ApJ*, **756**, 143
- Patsourakos, S., & Vourlidas, A. 2012, *SoPh*, **281**, 187
- Pesnell, W. D., Thompson, B. J., & Chamberlin, P. C. 2012, *SoPh*, **275**, 3
- Scherer, P. H., Schou, J., Bush, R. I., et al. 2012, *SoPh*, **275**, 207
- Schrijver, C. J., Elmore, C., Kliem, B., Török, T., & Title, A. M. 2008, *ApJ*, **674**, 586
- Smith, S. F., & Harvey, K. L. 1971, in *Physics of the Solar Corona*, ed. C. J. Macris (Dordrecht: Reidel), 156
- Srivastava, A. K., Zaqarashvili, T. V., Kumar, P., & Khodachenko, M. L. 2010, *ApJ*, **715**, 292
- Sterling, A. C., & Hudson, H. S. 1997, *ApJL*, **491**, L55
- Sturrock, P. A. 1966, *Natur*, **211**, 695
- Thompson, B. J., Plunkett, S. P., Gurman, J. B., et al. 1998, *GeoRL*, **25**, 2465
- Török, T., & Kliem, B. 2005, *ApJL*, **630**, L97
- Veronig, A. M., Muhr, N., Kienreich, I. W., Temmer, M., & Vršnak, B. 2010, *ApJL*, **716**, L57
- Wang, H., Liu, S., Gong, J., Wu, N., & Lin, J. 2015, *ApJ*, **805**, 114
- Wang, H., Shen, C., & Lin, J. 2009, *ApJ*, **700**, 1716

- Wang, Y.-M. 2000, [ApJL](#), **543**, L89
- Warmuth, A. 2007, in *Lecture Notes in Physics*, ed. K.-L. Klein, & A. L. MacKinnon, Vol. 725 (Berlin: Springer), 107
- Warmuth, A. 2015, [LRSP](#), **12**, 3
- Warmuth, A., & Mann, G. 2011, [A&A](#), **532**, A151
- Warmuth, A., Vršnak, B., Aurass, H., & Hanslmeier, A. 2001, [ApJL](#), **560**, L105
- Warmuth, A., Vršnak, B., Magdalenic, J., Hanslmeier, A., & Otruba, W. 2004a, [A&A](#), **418**, 1101
- Warmuth, A., Vršnak, B., Magdalenic, J., Hanslmeier, A., & Otruba, W. 2004b, [A&A](#), **418**, 1117
- White, S. M., Balasubramaniam, K., & Cliver, E. 2013, Air Force Research Laboratory, Tech. Rep., 22, 1
- Wills-Davey, M. J., & Attrill, G. D. R. 2009, [SSRv](#), **149**, 325
- Wills-Davey, M. J., DeForest, C. E., & Stenflo, J. O. 2007, [ApJ](#), **664**, 556
- Wu, S. T., Zheng, H., Wang, S., et al. 2001, [JGR](#), **106**, 25089
- Yuan, D., Pascoe, D. J., Nakariakov, V. M., Li, B., & Keppens, R. 2015, [ApJ](#), **799**, 221
- Zhukov, A. N. 2011, [JASTP](#), **73**, 1096
- Zhukov, A. N., & Auchère, F. 2004, [A&A](#), **427**, 705
- Zhukov, A. N., Rodriguez, L., & de Patoul, J. 2009, [SoPh](#), **259**, 73
- Zhukov, A. N., & Veselovsky, I. S. 2007, [ApJL](#), **664**, L131